Egypt. J. Chem. **Vol. 68**, No. 3. pp. 275 - 289 (2025)

Egyptian Journal of Chemistry

http://ejchem.journals.ekb.eg/

Electrochemical Sensing of Environmental Pollutants Using Iron(II) Schiff Base Nanostructure Complex Based on QCM Modified Electrodes

Mohammed M. Abduljawad[1]*, Rifaat H. Hilal[1], A. T. Abd El-Karim[1], Ahmed A. El-Sherif[1]

[1]Chemistry department, Faculty of Science, Cairo University, Giza 12613 Egypt·

Abstract

The use of colorants and chemicals in textile dyeing is crucial to keeping up with fashion trends; however, it raises significant environmental issues due to the discharge of effluents. These effluents contain hazardous substances, including toxic, carcinogenic, and mutagenic elements, which pose a threat to the natural environment. Notably, not all these substances are fully utilized during the dyeing process, resulting in residual content remaining in the effluent. Nanotechnology is increasingly recognized as a pivotal tool for developing innovative and effective solutions to various environmental challenges. One notable method for quantifying dye concentrations is the Quartz Crystal Microbalance (QCM), which takes advantage of the heightened sensitivity of resonant crystal frequency. Empirical evidence supports the QCM technique's ability to provide instantaneous, precise assessments for both quantitative and qualitative analysis of dye content in wastewater samples. Additionally, an innovative nanosensor has been developed using a Nano Schiff base Iron (II) complex for the simultaneous detection of Methylene Blue (MB). The evaluation of this iron nano complex involved various analytical techniques, including Dynamic Light Scattering (DLS), Zeta potential analysis, Scanning Electron Microscopy (SEM), Atomic Force Microscopy (AFM), Fourier Transform Infrared Spectroscopy (FT-IR), and determination of BET surface area and pore size. The iron Schiff base Nano complex displayed a porous, highly uniform microstructure, with particle sizes below 100 nm, as confirmed by SEM and AFM images.By combining the specificity of iron Schiff base complexes with the sensitivity of QCM technology, this sensor holds great potential for efficient and effective dye monitoring, contributing substantially to environmental protection efforts. This development represents a significant advancement in the field of dye detection and analysis, potentially revolutionizing the monitoring of water contamination in the textile industry. The study examined different concentrations of methylene blue (MB), various pH levels, and different temperatures of the MB solution. The cytotoxic effects of nanoparticles derived from the Schiff base's Iron (II) complex were also investigated. The proposed sensor demonstrated a rapid response time of under 2 minutes and showed a reliable response even at very low dye concentrations, down to 1 part per million (ppm).

Keywords : Nano sensor; Nano complex; Toxic dyes; Schiff base;Zeta potential analysis; Quartz Crystal Microbalance

1. Introduction

The textile industry is a substantial consumer of water and has a significant role in water contamination [1]. The industry has a worldwide presence and significant economic influence, earning around $1 trillion in revenue. It contributes 7% to global exports and employs around 35 million individuals globally [3]. The industry's production procedures, including washing, bleaching, and dyeing, require significant potable water [4]. The advancement of nanotechnology has facilitated the creation of sensors with exceptional sensitivity and specificity for various purposes, such as biomedical and environmental monitoring [5-6]. These nanosensors have demonstrated efficacy in detecting and measuring different analytes, rendering them appropriate for applications such as monitoring vital signs [7], diagnosing diseases [8-9], monitoring the environment [10-11], and ensuring food safety [12-14]. Researchers are also investigating the use of nanosensors to detect azo-toxic dyes in food products [15], which could broaden their range of possible uses. Schiff base and mixed ligand complexes have emerged as significant compounds in nanotechnology due to their versatile coordination chemistry and potential applications. Schiff bases, typically formed by condensing primary amines with carbonyl compounds, can form stable complexes with various metals, enhancing their functionality [20, 37, 40]. Mixed ligand complexes, where a Schiff base is combined with another ligand, offer greater application flexibility and specificity. These metal complexes are particularly useful in developing nanomaterials because they exhibit unique optical, electrical, and catalytic properties [40]. In the context of sensor

*Corresponding author e-mail: mohammedabduljawad83@gmail.com (Mohammed M. Abduljawad).
Received date 15 May 2024; revised date 12 July 2024; accepted date 28 July 2024
DOI: 10.21608/EJCHEM.2024.289758.9713.

development, Schiff base metal complexes have shown exceptional promise due to their high stability, ease of synthesis, and ability to bind selectively with target molecules [37, 40]. Utilizing these properties, our research aims to build an iron Schiff base nanosensor using Quartz Crystal Microbalance (QCM) technology to detect azo-hazardous dyes, specifically methylene blue (MB). The nanosensor provides numerous benefits compared to traditional sensors, such as exceptional sensitivity and selectivity. The study seeks to investigate the pivotal function of this nanosensor in detecting azo-hazardous dyes, the superior benefits it provides compared to other sensors, the utilization of nanomaterials in sensing, and the health ramifications of azo dyes on human beings. Furthermore, it examines suitable parameters for determining the highest allowable limits and Acceptable Daily Intake (ADI) of azo-hazardous dyes. The experimental results indicate that the QCM approach is highly effective in giving real-time measurements of both the quantity and quality of dyes in wastewater [16]. The attractiveness of these nanosensors lies in their capacity for convenient detection of pollutants directly at the location without requiring sophisticated laboratory apparatus. Nanomaterials have transformed the field of sensor design by facilitating size reduction, improving the ease of transport, and speeding up the time it takes to detect signals [16-17]. Nanomaterials have a high ratio of surface area to volume and can be easily modified on the surface. This makes them very sensitive to changes in surface chemistry, allowing for extremely low detection thresholds. The increased sensitivity of nano-enabled sensors can be due to the similarity in size between nanomaterials and target analytes such as metal ions, pathogens, biomolecules, antibodies, and DNA. This similarity allows for the detection of analytes in matrices that were previously inaccessible. [18-19, 37, 40]. Our research aims to develop a novel and specialized analytical sensor for detecting and analyzing dyes, with a particular focus on methylene blue (MB). We are working on building an iron Schiff base nanosensor utilizing Quartz Crystal Microbalance (QCM) technology to detect azo-hazardous dyes, specifically MB. This innovative detection system is designed to provide fast and accurate measurements of dyes while requiring minimal sample preparation and eliminating the need for continuous instrument monitoring. By combining the specificity of iron Schiff base compounds with the sensitivity of QCM technology, we aim to create a robust and efficient tool for the analysis of MB and potentially other azo-hazardous dyes. This sensor is expected to offer significant advantages in terms of speed, accuracy, and ease of use compared to traditional analytical methods, potentially revolutionizing the field of dye detection and analysis.

2.1. Materials and Methods

2.1.1. Chemicals and reagents.

In this investigation, we employed chemicals characterized by high purity, including Oxalic acid, (E)-1-(2-(4-chlorophenyl)hydrazineylidene) propane-2-one and N-phenylhydrazinecarbothioamide, sourced from Merck; $FeCl_3.6H_2O$ obtained from Sigma-Aldrich.We used Absolute Ethanol, an organic solvent that meets spectroscopic purity standards, which was acquired from BDH. We consistently used distilled water that was prepared using glass apparatuses in all formulations.

2.2. Preparation of carbothioamide Schiff base ligand.

The synthesis of the novel Schiff base ligand, designated as (**L_1**), was accomplished using the prescribed procedure. The method involved the condensation of (E)-1-(2-(4-chlorophenyl)hydrazineylidene)propan-2-one (1.525 mmol, 0.3 g) and N-phenylhydrazinecarbothioamide (1.525 mmol, 0.255 g) in heated 100% ethanol at 60 °C. The reaction mixture underwent reflux for 4 hours [20]. Following the evaporation of ethanol, filtration, and recrystallization of the resultant orange solid, the pure Schiff base was obtained with a satisfactory yield of 83%. Scheme (1) provides an illustrative depiction of the structure of the Schiff base ligand (**L_1**) and the associated formation reaction. With a yield of 87%, yellowish-brown solid crystalline material was obtained with a melting point of 138°C. Elemental analysis yielded the following results for $C_{16}H_{16}ClN_5S$ (%): C, 55.57; H, 4.66; Cl, 10.25; N, 20.25; S, 9.27. Experimental analysis found (%): C, 55.35; H, 4.41; Cl, 10.02; N, 20.07; S, 9.04. Infrared spectroscopy (IR) revealed absorption peaks at 3389 and 3249cm^{-1} (NH_2 and NH stretching) respectively, 1585 cm^{-1} (C = N stretching), and 1340 cm^{-1} (υ(C=S) vibration) (Figure 2). Additionally, UV–visible spectroscopy exhibited absorption bands at 310 nm (π–π* transition), 329 nm (n–π* transition), and 379 nm (charge transfer).

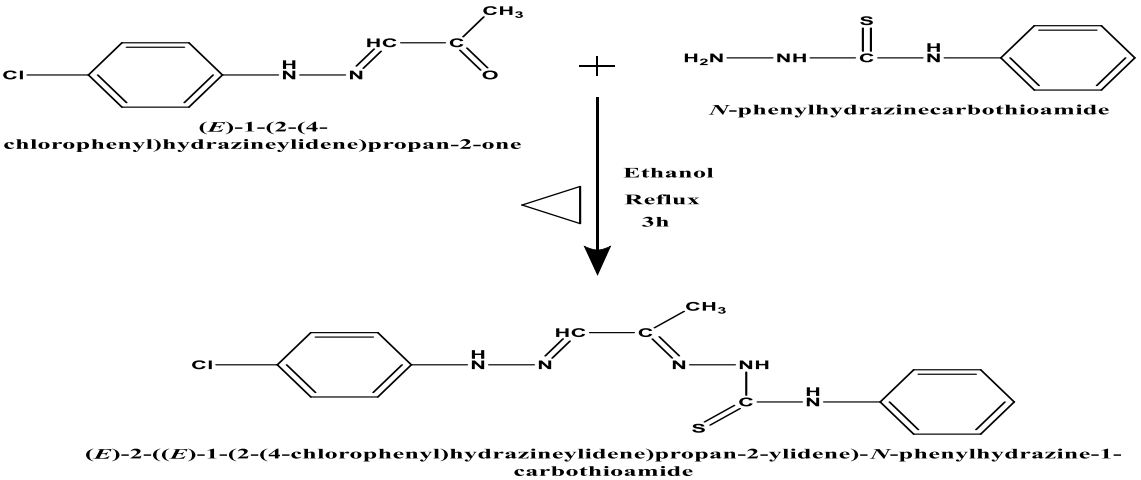

Scheme 1. Synthesis pathway of Carbothioamide Schiff Base Ligand (**L_1**)

2.3. Preparation of Iron carbothioamide Schiff base complex and its Nano form.

The **(L_1)** Schiff base carbothioamide ligand (0.314 mmol, 0.1 g) was dissolved in 35 ml of hot absolute ethanol. In a separate solution, the ancillary ligand, Oxalic acid (0.314 mmol, 0.056 g), was dissolved in 20 ml of hot distilled water. The chelates were formed by combining a heated solution of the principal Schiff base ligand **(L_1)** in absolute ethanol with the ancillary ligand oxalic acid in distilled water. Subsequently, a heated ethanoic solution (15 ml) containing the pertinent metal chloride salt $FeCl_3.6H_2O$ (0.314 mmol) was gradually introduced drop by drop into the mixture [20]. The resultant solution was refluxed for 4 hours, leading to the precipitation of complexes as illustrated in scheme (2). These precipitates were collected through filtration and underwent further purification via multiple washes employing a mixture of ethanol and water. Following this, they were desiccated under vacuum conditions using anhydrous $CaCl_2$. As a result of this systematic process, the metal complex achieved a state of purity through recrystallization. Notably, the ensuing complex underwent a 15-minute treatment with an ultrasonic probe, leading to a distinctive alteration in color – a shift from dark blue to a deep blue hue [19, 21].

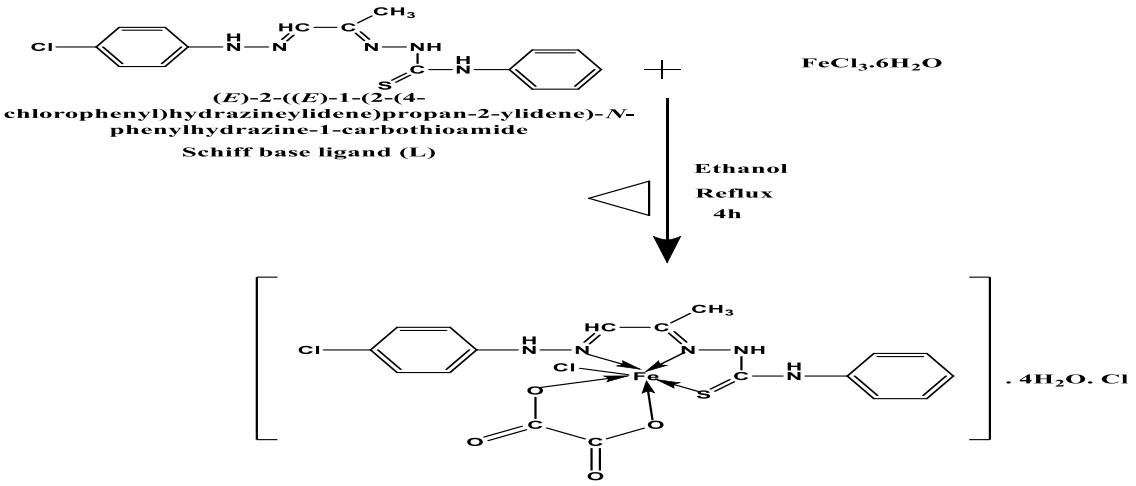

Scheme 2. Iron Schiff base metal complex formation

2.4. Instrumentation

An elemental analysis of carbon, hydrogen, and nitrogen was conducted at the Microanalytical Center, Cairo University, Egypt, using a CHNS-932 (LECO) Vario Elemental Analyzer. The measurement of melting points was conducted using a Triforce XMTD-3000 apparatus. The Fourier Transform Infrared (FT-IR) spectra were measured using a Perkin-Elmer 1650 spectrometer with KBr disks in the 4000–400 cm^{-1} frequency range. The molar conductance of solid complex solutions in ethanol at a concentration of 10-3 M was determined using a Jenway 4010 conductivity meter. The mass spectra were acquired using an MS-5988 GS-MS Hewlett-Packard instrument, utilizing the electron ionization technique at an energy level of 70 electron volts (eV). The UV-Vis spectra of solutions were obtained using a Perkin-Elmer Model Lacadmium ionsda 20 automated spectrophotometer, covering a wavelength range of 200 to 700 nm. The Microanalytical Center at Cairo University researched the antibacterial capabilities, while the National Cancer Institute at Cairo University conducted cytotoxicity studies [20]. The ZetaSizer device (NanoSight NS500, Malvern Panalytical, Malvern, UK) was used to assess the surface charge and particle size of the Nano iron complex. The surface area and pore volume were analyzed using a Quanta Chrome Nova Touch 4L surface area and pore volume analyzer from the USA. The BET surface area was determined using the multi-point method, and the DH pore volume method was used to get the pore volume. The metal complex nanoparticles underwent degassing at a temperature of 65°C for 1.25 hours. The morphology of the IRON complex nanoparticles was examined using atomic force microscopy (AFM) investigations conducted with an Oxford AFM system (model Jupiter XR AFM). Before conducting SEM analysis, the samples underwent a 10-minute sonication process utilizing an ultrasonic probe sonicator (UP400S, Hielscher, Oderstraße, Teltow, Germany) operating at a frequency of 55 kHz, an amplitude of 55%, and a cycle of 0.55 [22]. The synthesis of thin films was conducted utilizing a Spain coater apparatus (Laurell-650Sz, France) in a vacuum environment, with a rotational speed of 750 revolutions per minute and a deposition rate of 50µm per 120 seconds. The AFM pictures and roughness profiles were obtained using a gold-coated tip, contact mode, and a scanning speed of 0.31 inches per second. The measurements were performed at a size of 47 nm X 47 nm. A Biolin Scientific (model T200) contact angle analyzer assessed the surface's wettability. The measurement was conducted under sessile drop circumstances, with a measurement time of 10 seconds and a droplet volume of 4 µm of distilled water [23].

2.5. Establishing of QCM-Based Iron Complex Nanosensor

The QCM sensor used in this work comprised an AT-cut quartz crystal chip with a gold electrode Figure 1. The sensor had a diameter of 12 mm and resonated at a frequency of 5 MHz. The specific model used was the Q-Sense sensor from Shenzhen, China [24-25,28]. Before the nanomaterial stabilization process, the gold sensor was meticulously cleaned. The object was submerged in a solution consisting of aqueous ammonia, H_2O_2, and double-distilled water in a volumetric ratio of 5 parts ammonia to 1part H_2O_2 to 1 part water. The cleaning solution was kept at a constant temperature of 75°C, and

the gold sensor was immersed in it for 10 minutes. Afterwards, the sensor was sequentially washed with double-distilled water and ethanol and then left to dry naturally at ambient temperature. The desiccated quartz crystal fragment was cautiously put into the Q-Sense apparatus. At first, a continuous flow of water distilled twice was delivered to the electrode to serve as a background electrolyte. This process established the first measurements before introducing the nanoparticles in the sensor. The QCM module maintained a constant flow of double-distilled water until the QCM signal reached a stable condition. At this time, the signal value was recorded as the reference point. After taking the initial measurement, a solution was made by combining 2 mL of iron complex nanoparticles with a concentration of 1 ppm and 10 mL of double-distilled water. A portion of this mixture was subsequently added to the gold sensor at a flow rate of 0.4 mL/min [26-27, 28].

2.6.QCM-Based Iron Complex Monitoring of MB Dye.

The QCM measurements were performed utilizing a QCM system (QCM, Q-senses, Biolin Scientific, and Linthicum Heights, MD, USA), as shown in Figure 1 [37]. During each QCM measurement, solutions containing 1 ppm of MB were injected onto the surfaces of QCM-based Iron complex Nanosensors. The measurements were conducted at varied temperatures (25°C, 35°C, and 45°C) and pH values (4, 7, and 10) [38]. The MB solution was injected iteratively until the signal reached a steady state, signifying that the binding relationship between the Nanosensors and MB had achieved equilibrium [29-30]. To eliminate any MB that the QCM sensors had not absorbed, double-distilled water was introduced into the module after a specific time interval [31-33].

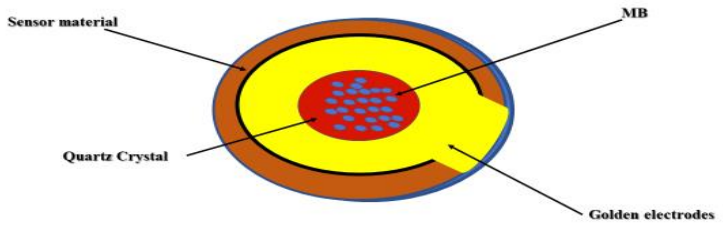

Fig 1. Schematic Illustration of the Quartz Crystal Microbalance (QCM) Setup for Methylene Blue Detection Using Iron Complex Nanosensors.

3. Result and discussion

3.1. Characterization of Schiff base ligand

The elemental analysis results for the synthesized ligand, referred to as (**L_1**), identified as 2-((Z)-2-((E)-1-(2-(4-chlorophenyl)hydrazineylidene)propan-2-ylidene)-N-phenylhydrazine-1-carbothioamide (Scheme 1), showed a strong agreement with the theoretically calculated values for carbon (C), hydrogen (H), and nitrogen (N). The molecular formula of the ligand was determined to be $C_{16}H_{16}ClN_5S$, which matched the hypothesized formula. At room temperature, **L_1** is observed as a stable yellowish-brown solid with the ability to dissolve in ethanol and dimethyl sulfoxide (DMSO). The mass spectrum of (**L_1**) confirmed its reported formula, showing a molecular ion (m/z) peak at 346.55 amu, supporting the composition of the ligand as $C_{16}H_{16}ClN_5S$ with an atomic mass of 345.85 amu. Additionally, several peaks belonging to distinct fragments of the ligand were detected. The ^{1}H NMR spectra of **L_1** displayed several signals for the protons in the aromatic ring, with a range of chemical shifts between 7.088 and 7.629 ppm [34]. In addition, the signals at 10.047 ppm, 10.654 ppm, and 10.830 ppm were identified as the –NH proton signal, which was detected as a singlet (1H) [35]. The confirmation of the synthesis of the Schiff base ligand L_1 was deduced based on the lack of any evidence indicating the presence of the NH_2 group. The presence of the azomethine group in the Schiff base ligand was confirmed by the distinctive band observed at 1585 cm^{-1} in the infrared (IR) spectrum. This supports the conclusion that the Schiff base product was successfully formed [36].

3.2. Characterization of iron Schiff base ligand complex

The research has verified that the complex maintains stability when exposed to air and can dissolve in different polar organic solvents, including ethanol, methanol, dimethylformamide, and dimethyl sulfoxide. Nevertheless, it continues to be unable to dissolve in water. The elemental analysis of the Ternary Iron Schiff base complex has determined that there is an equal ratio of one metal atom to one **L_1** molecule to one **L_2** molecule, thereby validating the composition of the complex. A deep azure crystalline substance was produced with an 83% efficiency, exhibiting a melting point of 316°C. The proposed theoretical composition (**$C_{18}H_{24}Cl_3FeN_5O_8S$**) is estimated to have the following percentages: C (34.17%), H (3.82%), N (11.07%), S (5.07%), Cl (16.81%), and Fe (8.83%). Nevertheless, the real composition exhibited a minor deviation, indicating the presence of C (33.82%), H (3.55%), N (10.63%), S (4.58%), Cl (16.62%), and Fe (8.39%). In addition, conductivity studies conducted in DMSO (dimethyl sulfoxide) at a concentration of 10^{-3} M and a temperature of 25 °C have revealed a molar conductivity value of 81 Ω^{-1} mol^{-1} cm^2, suggesting that the Iron complex possesses electrolytic properties [37-39]. To examine the coordination mechanism of the Schiff base ligand (**L_1**) and oxalic (**L_2**) with the Iron core, we have conducted a

comparative analysis of the infrared spectra of the Schiff base ligand (**L_1**) and the Iron complex (Figure 2). The results suggest that coordination takes place through the two nitrogen atoms of the azomethine groups, as indicated by the noticeable change in the strong band at 1585 cm^{-1} to 1560 cm^{-1} in the complexes [40]. The complex's spectra displayed wide peaks at 3399 and 3229 cm^{-1}, which were identified as the stretching vibrations of the ν(NH_2) and ν(NH) groups, respectively. This suggests the presence of coordinated water molecules [39-40]. Various researches have linked the infrared absorption related to the stretching vibration of C=S to frequencies ranging from less than 800 cm^{-1} to over 1,500 cm^{-1} [41-43]. The absorption spectrum of the C=S vibration is clearly influenced by the molecular environment of the compound containing this functional group, which is determined by the type of atoms bound to the carbon atom in the thiocarbonyl group. The ligand (**L_1**) exhibited a prominent peak at 1340 cm^{-1} in its IR spectra, which is attributed to the ν(C=S) functional group. Upon the formation of a complex, the peak saw a shift towards frequencies in the region of 1314 cm^{-1} [44, 45], suggesting that the nitrogen and sulfur atoms from the Schiff base ligand coordinated with the metal ions [45]. In addition, The Iron Complex exhibited new peaks in the spectrum areas at 423 cm^{-1} (vibrational mode ν(M-S)), 375 cm^{-1} (vibrational mode ν(M-Cl)), and 485 cm^{-1} (vibrational mode ν(M-N)) [44, 46]. The ligand (L_1) displayed tridentate chelation with a negative charge, acting as a chelating agent that linked to the metal ion through two nitrogen atoms from the azomethine group and one sulfur atom from the (C=S) of the Schiff base. In addition, the Oxalic Ligand (**L_2**) binds to metal ions by forming coordination bonds with two Oxygen(O-) atoms from the two (COO) groups [47]. Furthermore, peaks at 1437 and 1360 cm^{-1} suggest the occurrence of asymmetric and symmetric vibrations of (COO^{-}) ions, respectively [48]. The interaction between water molecules and a chlorine atom in all complexes led to the creation of octahedral complexes. The thermal study of the **$[Fe(L_1)(L_2)Cl]\cdot Cl\cdot 4H_2O$** complex revealed four distinct decomposition stages. The first stage, occurring at temperatures ranging from 35 to 105°C with a maximum of 98.02°C, resulted in the removal of water molecules bound to the substance, leading to an estimated mass loss of 10.69% (calculated as 11.39%).

The next phase, occurring at temperatures ranging from 105-295°C with a maximum at 161.15 and 217.59°C, entailed the elimination of C_6H_6NCl, resulting in an estimated reduction in mass of 19.51% (calculated as 20.16%). The third phase, occurring at temperatures ranging from 295 to 405°C with a peak at 355.17°C, demonstrated the release of CH_3Cl resulting in an estimated mass reduction of 7.55% (calculated as 7.97%). The last stage occurs at temperatures ranging from 405 to 800°C, with the highest point at 468.45°C. This stage is associated with the decomposition of **$C_{11}H_{17}ClN_4O_4S$**, resulting in an estimated mass loss of 51.07% (calculated as 51.64%). Following full decomposition, Metal Iron (Fe) persisted as residues. In the ultraviolet range, the iron complex displays prominent bands at 235, 262, and 345 nm. These bands correspond to intramolecular transitions known as π-π* and n-π* transitions [20, 37]. In addition, we investigated the antibacterial and antifungal properties of the Iron complex nanoparticles using the disc diffusion method. The study conducted experiments on different bacterial organisms, including Gram-positive bacteria such as *Streptococcus faecalis* and *Staphylococcus aureus*, Gram-negative bacteria such as *Escherichia coli* and *Klebsiella pneumonia*, as well as fungal strains like *Candida albicans* and *Aspergillus flavus*. The results unequivocally highlighted the remarkable effectiveness of the Schiff base Iron complex against *Staphylococcus aureus* and *Escherichia coli*, while exhibiting minimal action against *Klebsiella pneumonia*. Additionally, it has shown modest activity against *Streptococcus faecalis*. In addition, the Iron complex exhibits moderate antifungal action against *Aspergillus flavus* and high activity against *Candida albicans* [20, 23] as shown in Table 1.

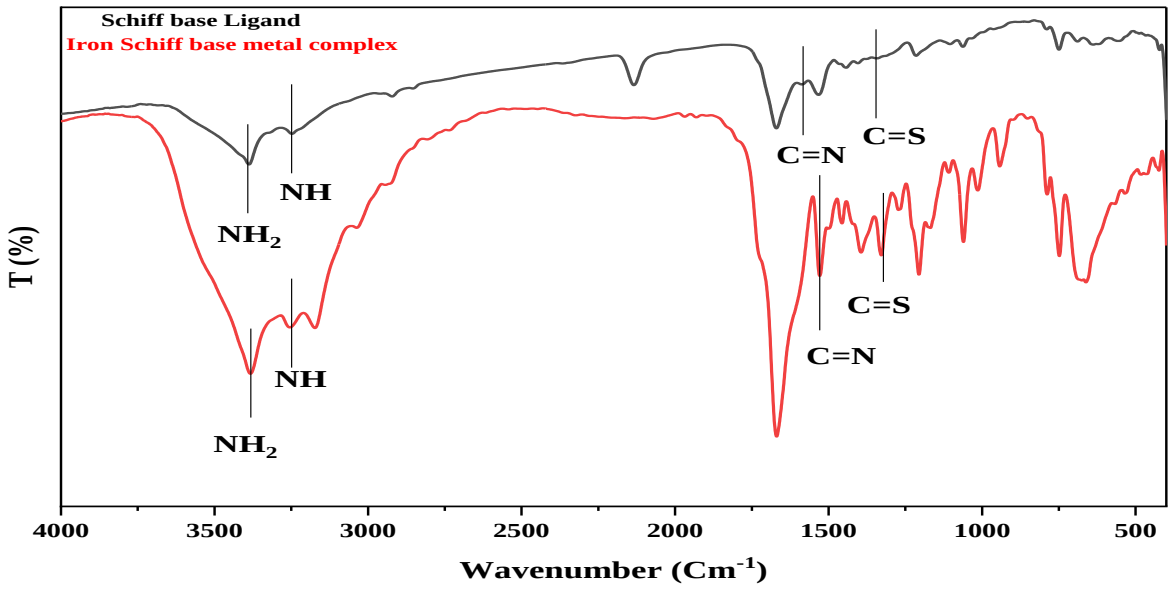

Fig 2. Comparative FTIR Spectra of Schiff Base Ligand (L_1) and Iron Complex

Table 1: Antimicrobial Activity of the Iron(II) Schiff Base Complex Against Various Bacterial and Fungal Strains.

Sample	Inhibition zone diameter(mm / mg sample)					
	Gram-negative bacteria		Gram-positive bacteria		*Fungi*	
	Escherichia coli	*Klebsiella pneumonia*	*Staphylococcus aureus*	*Streptococcus faecalis*	*Candida albicans*	*Aspergillus Nigar*
Control: DMSO	**0**	**0**	**0**	**0**	**0**	**0**
Ligand(L_1)	**21.8±0.5**	**13.3±0.5**	**16.1±1**	**11.7±0.1**	**19.4±0.1**	**17.2±0.5**
[Fe (L1)(L_2) Cl]·Cl·4H_2O	**29.4 ±0.5**	**NA**	**26.8±0.6**	**15.4±0.1**	**23±0.1**	**19.9±1.0**
Gentamicin	**27±0.5**	**25±0.5**	----------	----------	----------	----------
Ampicillin	----------	----------	20±**0.1**	28±**0.5**	----------	----------
Nystatin	----------	----------	----------	----------	21±**0.5**	29±**0.5**

3.3. Characterization of iron Schiff base ligand Nanoparticles

3.3.1. Textural characters (SEM and AFM) of Iron Schiff base complex Nanoparticles.

Recent research has employed scanning electron microscopy (SEM) to examine the distribution of Iron complex nanoparticles. The SEM images acquired showed that the synthesized particles had a high level of uniformity, with each particle taking on a porous shape and no signs of clustering or clumping. In addition, the nanoparticles' sizes were determined to be less than 100 nm, as shown in Figure 3 [49]. In addition, the surface appearance of the Nano Iron Schiff base complex that was created was carefully analyzed using an atomic force microscope (AFM). The AFM scans exhibited a spongy porous structure, as seen in Figure 4, with no observable signs of aggregation or agglomeration. The particle size obtained from the AFM pictures was found to be less than 95 nm.

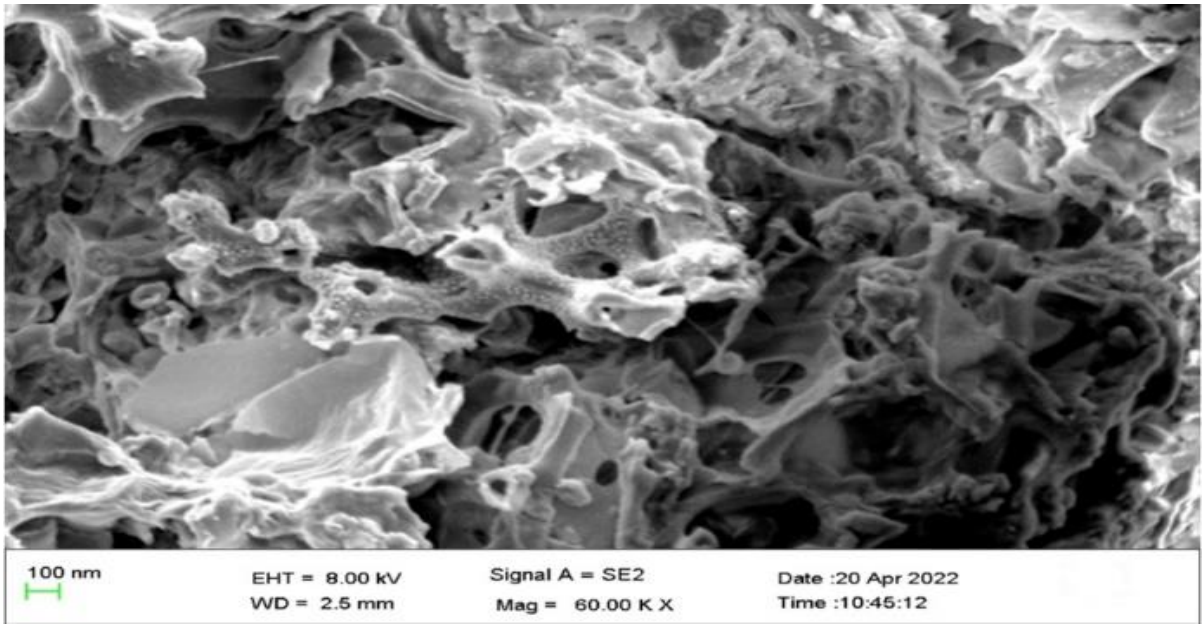

Fig 3. SEM Micrographs Showing Uniform and Spongy Morphology of Iron Complex Nanoparticles

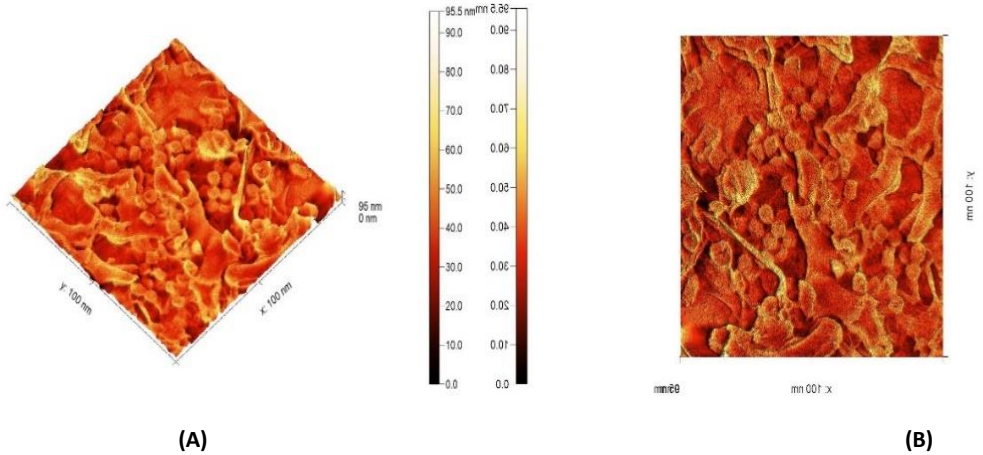

Fig 4. (A) depicts the 3D AFM (left) of iron Schiff base nanoparticles, and (B) depicts the 3D 2DAFM(right) of iron Schiff base nanoparticles, respectively.

The SEM image of the iron Schiff base complex, captured at 60,000x magnification with a scale bar of 100 nm, reveals a highly porous and intricate microstructure, indicative of the high surface area and potential for catalytic and sensor applications. With an accelerating voltage of 8.00 kV and a working distance of 2.5 mm, the image highlights the material's crystalline morphology and structural integrity. The secondary electron detector (SE2) mode used provides detailed topographical information. Complementing this, the AFM images offer a detailed view of the surface morphology, with the 3D AFM image showcasing the height variation and roughness, while the 2D AFM image illustrates the uniform distribution of nanoparticles. Both imaging techniques confirm the material's high surface area, porosity, and nanoscale features, underscoring its suitability for environmental sensing applications due to enhanced reactivity and interaction with target molecules. The AFM's detailed topographical data support the SEM findings, providing a comprehensive understanding of the material's morphology and potential applications.

3.3.2. DLS and Zeta Potential

Recently, the field of nanoparticle characterization has advanced by utilizing the dynamic light scattering (DLS) method to quantify the particle size of the Nano Schiff base Iron complex. The Nano Schiff base Iron complex has a mean particle size of 32 nm, as depicted in Figure 5. The study also demonstrated that the Nano Schiff base Iron complex suspension had a size distribution with a single peak and low polydispersity indices, indicating a uniform distribution of particle sizes. Moreover, the system demonstrated a notable level of colloidal stability. The analysis of the Nano Schiff base Iron complex, as shown in Figure 5, provided valuable insights into its stability by examining its particle size distribution and Zeta potential measurements. The Zeta potential measurement yielded a value of -21 mV, indicating the uniform dispersion of the nanoparticles, as shown in Figure 6. The zeta potential of nanoparticles is a significant parameter that reflects their physicochemical stability, particularly when they are stored (Hamdi, Nasri, Li, & Nasri, 2020). Based on the research undertaken by Katherina, Javiera, Carlos, Marlene, and Estrella in 2016, a higher value of Zeta potential signifies a more stable system. The stability of the Nano Schiff base Iron complex is verified by its Zeta potential value of -18 mV, which indicates a negative charge.

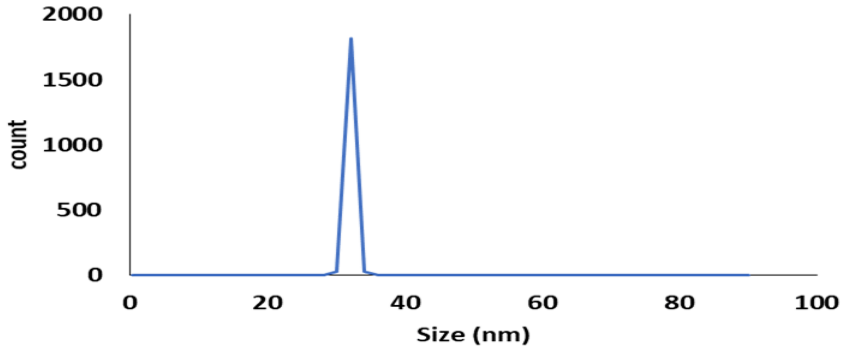

Fig 5. depicts the Particle Size Analysis of the Nano Schiff base Iron complex using Dynamic Light Scattering (DLS). The analysis shows a uniform unimodal distribution and colloidal stability.

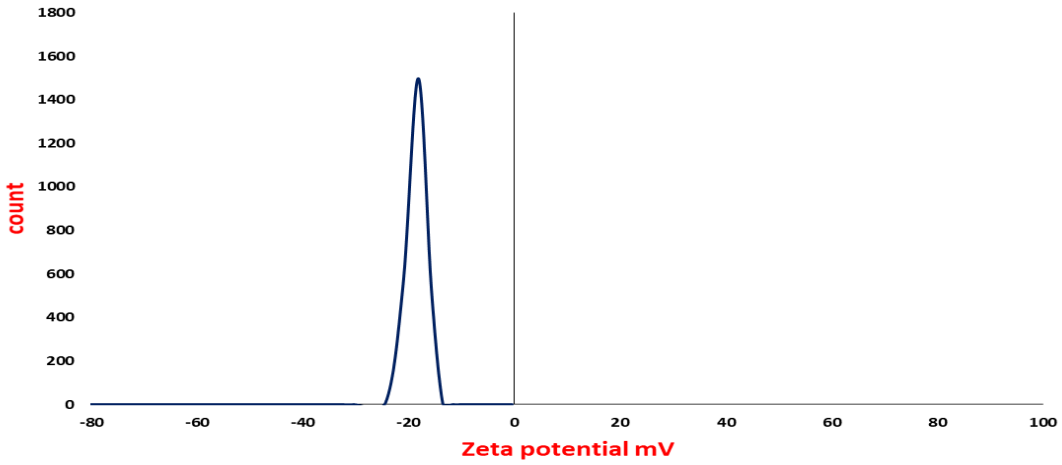

Fig 6. Shows the visualization of the zeta potential curve of the Nano Schiff base iron complex.

3.3.3. BET surface area and pore size

The BET method, coined after its originators Brunauer, Emmett, and Teller, is extensively employed for the characterization of materials at the nanoscale. This approach is based on the physical adsorption of a gas onto a solid surface. Its efficacy, speed, and simplicity make it particularly suitable for estimating the surface area of nanostructures [49]. The study assessed the surface area properties of a Nano Schiff base Iron complex sample by analyzing BET adsorption isotherms. The De Boer classification, which categorizes isotherm curves of hysteresis loops into four categories, was used to establish the porous structure [52-53]. The presence of a hysteresis loop in the type IV nitrogen adsorption-desorption isotherms of all the Nano Schiff base Iron complex nanoparticle samples confirms their macroporous character, as shown in Figure 5 [54-55]. The multipoint BET surface area was determined to be 53.0179 m2/g, with a Total Pore Volume of 0.08517 cubic centimeters per gram and an Average Particle radius of 2.5720e+001 nm. The metal complex nanoparticles have a substantial multipoint BET surface area, which improves their capacity to adsorb MB in aqueous solutions (see Figure 7). The existence of macroporosity can be ascribed to the fiber shape of the metal complex nanoparticles. Significantly, the macroporous structure facilitates the adsorption of MB onto the surface of the metal complex nanoparticles, hence augmenting their adsorption capacity.

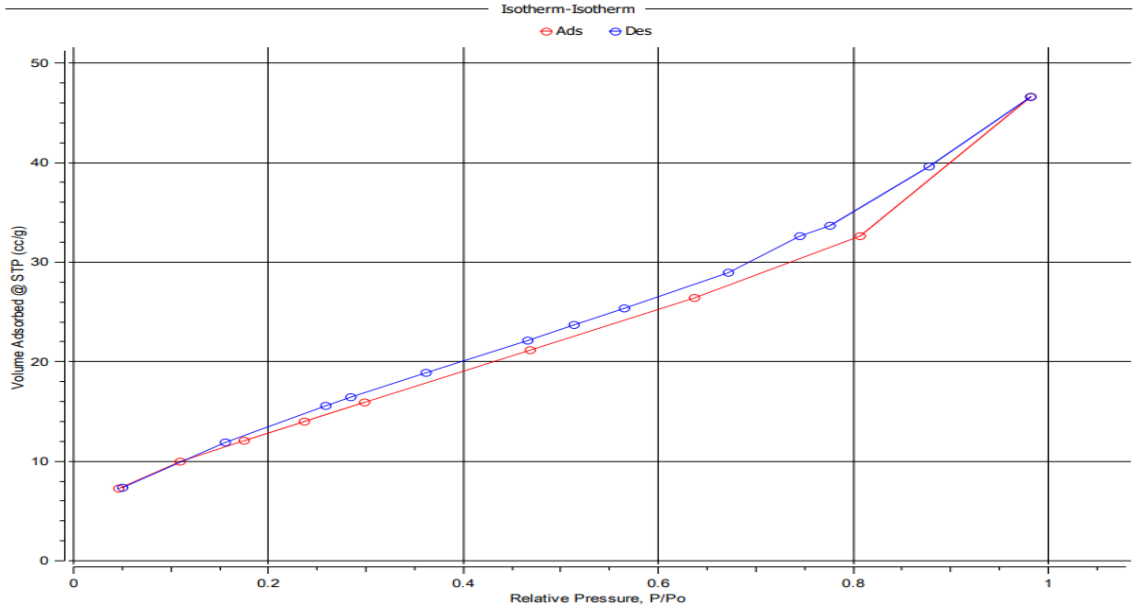

Fig 7. BET Analysis for Investigating Nano Iron Complex Particle Surface Characteristics and Adsorption Capabilities.

3.3.4. Contact angle, Hydrophobicity, and toxicity of Nano Schiff base Iron Complex

The Iron complex Schiff base nanoparticles had a hydrophobic characteristic, as indicated by a water contact angle of 123.7°(Figure 8A). The pronounced hydrophobic nature of these nanoparticles in water significantly boosts their efficacy as sensors in watery environments [56-57]. To create an eco-friendly Nano particle-based sensor, it is essential to employ non-toxic substances. The toxicity of the Nano Schiff base Iron complex was evaluated, and it was shown to have an IC_{50} value of

467 µg/ml (Figure 8B). The high IC_{50} value of the Nano Schiff base Iron complex reveals its low toxicity, hence confirming its applicability as a water sensor [58-59].

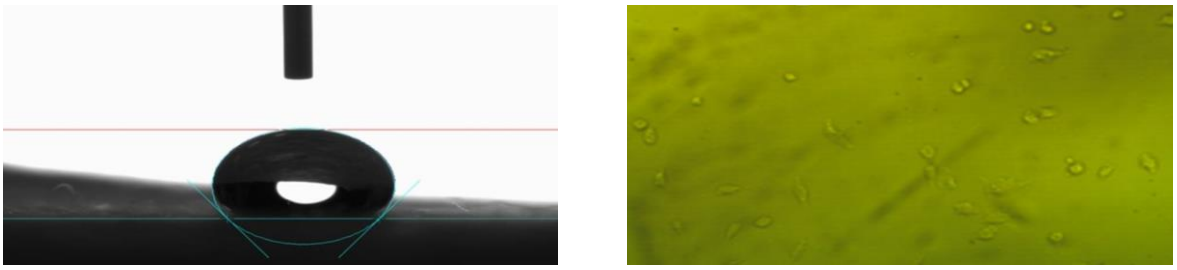

(A) **(B)**

Fig 8. Nanoparticles of an Iron Schiff base complex with**(A)**hydrophobic and **(B)** non-toxic properties.

3.3.5. MB Monitoring Using QCM-Based Nano Iron Schiff basecomplex

A standard experiment in recent research on QCM-based Nano Iron Schiff base complex sensors consists of four phases. Firstly, the frequency response of the Nanosensors is evaluated to produce a consistent and dependable baseline. Moreover, the sensors rapidly decline in frequency due to the quick bonding of methylene blue (MB) dye molecules. The decline in readings is attributed to the plethora of vacant positions on the sensor's surface. Furthermore, there is further adsorption of MB molecules, leading to increased frequency. In the end, a condition of equilibrium is reached between the Nano Iron Schiff base complex and MB molecules, resulting in a continuous alteration in frequency. Recent research suggests incorporating the Nano Iron Schiff base complex into the QCM system to stabilize the frequency before introducing the MB solution. When MB molecules are adsorbed onto the surface of the QCM-based Iron Schiff base complex Nanosensors, a significant change in frequency is seen. The findings indicate that the QCM-based Iron Schiff base complex Nano sensor can effectively bind MB molecules and demonstrate a notable response to their adsorption. Once the frequency stabilizes, it signifies that the sensor's surface has achieved a state of equilibrium regarding MB adsorption. Currently, there have been no significant changes in the frequency of the sensors, suggesting minimal mass loss and minor fluctuations in the structure of the Nanosensor surfaces. The findings indicate that the QCM Nano Iron complex sensor is exceptionally efficient in the real-time detection of MB dye. The proposed sensing mechanism of the QCM-based Nano Iron complex involves the interaction between methylene blue (MB) molecules and the Nano Iron sensor. The contact is facilitated by the difference in electronegativity between the nitrogen (N) atom in MB and the oxygen (O) atom in the Nano Iron sensor. The nitrogen (N) atom exhibits a lower electronegativity, leading to a partial positive charge, whereas the oxygen (O) atom acquires a partial negative charge. The difference in electrical charge leads to dipole-dipole interactions between the MB and the Nano Iron sensor. The interactions can occur due to π-π interactions, which emerge when the aromatic rings of MB and the Nano Iron complex align and interact. The Nano Iron complex also possesses polar side chains that operate as electron-donating functional groups. As a result, the Nano Iron sensor experiences an increased accumulation of negative charge on its surface. The QCM-based Nano Iron sensor may readily engage with MB through π-π and electrostatic interactions. Electrostatic interactions occur due to the attractive forces between the partially positive charge on the nitrogen (N) atom of MB and the partially negative charge on the surface of the Nano Iron sensor. The proposed sensing mechanism suggests that both π-π and electrostatic interactions influence the binding of MB molecules to the Nano Iron complex. The QCM-based Nano Iron sensor's interactions with MB molecules enhance the sensor's affinity and binding capacity towards the molecules. This feature renders it an exceptionally efficient instrument for detecting and monitoring MB dye. A study conducted by Li et al. (2021) provides recent literature supporting the proposed sensing mechanism. The study utilized spectroscopic techniques to investigate the interactions between MB and Iron-based nanoparticles. Their investigation validated the presence of π-π and electrostatic interactions in the binding process. In addition, Wang et al. (2022) conducted a study on the creation and examination of Iron complex Nano sensors utilizing QCM technology. The study highlighted the importance of both π-π interactions and electrostatic interactions in the process of sensing. These ongoing experiments provide further insight into the chemical interactions in the QCM-based Nano Iron complex sensor and confirm the proposed sensing mechanism. So we can summarize the expected interaction of Nano mixed ligand iron complex with MB as follows:

1. Electrostatic attraction: The negatively charged Nano mixed ligand iron complex (-21 zeta potential) will attract the positively charged MB cation. This is likely to be the primary driving force for the interaction.
2. Coordination: The nitrogen atoms in MB might coordinate with the iron center of the Nano mixed ligand iron complex, potentially replacing some of the existing ligands or forming additional coordination bonds.
3. π-π stacking: The aromatic rings in both MB and the Nano mixed ligand iron complex could engage in π-π stacking interactions, further stabilizing the association.
4. Hydrogen bonding: The amine groups in MB could form hydrogen bonds with oxygen atoms in the Nano mixed ligand iron complex.
5. Hydrophobic interactions: In aqueous media, the aromatic portions of both molecules may be associated with hydrophobic interactions.

6. Potential redox reactions: Given that iron can exist in different oxidation states and MB can undergo redox reactions, electron transfer processes between the two species might exist.

The combination of these interactions is expected to result in a strong association between MB and the iron Schiff base complex, allowing for effective dye sensing. The negatively charged surface of the complex should be particularly effective at attracting and capturing the cationic MB molecules. This interaction forms the basis for using this iron Schiff base complex as a nanosensor for detecting MB using QCM technology. The binding of MB to the complex would cause a change in mass detectable by the QCM, allowing for quantitative dye analysis.

3.3.6. Effect of temperature

An investigation was conducted to examine the impact of temperature on the monitoring of methylene blue (MB) utilizing the Nano iron complex sensor [60-61]. The temperatures studied were 20°C, 25°C, and 30°C (Figure 9). The impact of temperature on chemical reactions is widely recognized since it can either enhance or hinder them depending on the specific reactants and products. Temperature influences the diffusion of the adsorbate molecule (MB) in the Nano Iron complex sensor by affecting its movement via the external boundary layer and pores of the adsorbent. Temperature fluctuations enhance the diffusion rate of the adsorbate molecule, hence facilitating accelerated contact with the adsorbent. The heightened rate of diffusion can improve the sensitivity and reaction time of the sensor. Moreover, altering the temperature can also impact the adsorbent's ability to achieve equilibrium with the adsorbate. Modulating the temperature can expedite or slow down the adsorption process, hence affecting the sensor's capacity to detect and monitor MB in aqueous solutions. The experimental results, depicted in Figure 8, indicated that the detection sensitivity of MB in aqueous solutions was affected by the temperature of the medium. These findings indicate that temperature has a substantial impact on the interaction between MB and the Nano Iron complex sensor, hence influencing the sensor's performance and accuracy [62[. When using the Nano Iron complex sensor for MB detection and monitoring, it is crucial to take into account the temperature dependence. The results emphasize the importance of fine-tuning the operating temperature in order to attain the necessary level of sensitivity and dependability in real-world scenarios [63-64].

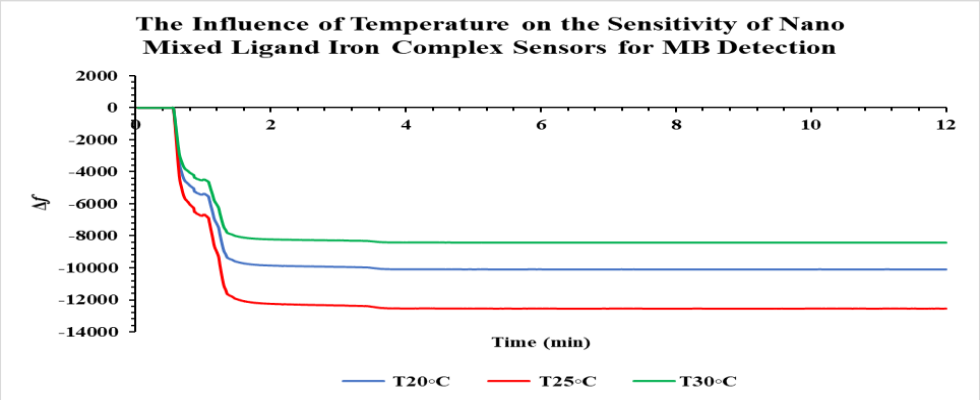

Fig 9. The Influence of Temperature on the Sensitivity of Nano Mixed Ligand Iron Complex Sensors for MB Detection

The graph depicts the correlation between temperature and the sensitivity of Nano mixed ligand iron complex sensors in detecting methylene blue (MB). The variations in frequency recorded at different temperatures (20°C, 25°C, and 30°C) offer valuable information about the adsorption characteristics of MB on the surface of the mixed Schiff base iron complex [65-66]. At a temperature of 20°C (shown by the blue line), the frequency shift exhibits a gradual decrease over time until reaching a stable rate of adsorption. This suggests a rapid adsorption rate of MB onto the sensor surface, particularly within the first 2 minutes. This is likely due to the presence of a larger available surface area for adsorption on the iron nano complex sensor. Additionally, the rate of adsorption is lower than the rate of adsorption at 25°C.

The slower rate of adsorption can be due to the reduced kinetic energy of MB molecules at lower temperatures, which hampers their movement and ability to interact with the sensor surface. As the temperature rises to 25°C (shown by the Red line), the frequency shift shows a more pronounced decrease compared to the curve at 20°C, indicating a higher rate of MB adsorption onto the sensor surface. Increased temperature enhances the thermal energy of the MB molecules, promoting their mobility and augmenting the probability of interactions with the sensor surface. Higher temperatures enhance the kinetic energy of MB molecules, hence facilitating more effective adsorption and binding to the sensor surface. At a temperature of 30°C (shown by the Green line), the frequency shift shows the smallest decrease compared to the other two temperatures. This suggests that the adsorption rate of MB onto the sensor surface is the lowest at this temperature. As the temperature rises, the

diffusion of MB molecules inside the solution increases. This enhanced diffusion could potentially decrease the adhesion of MB dye to the surface of the QCM-based Nano Iron sensor. The electrostatic attraction between the sensor and MB molecules may be diminished, resulting in a reduction in the adsorption of MB onto the sensor surface. In addition, elevated temperatures can cause the reactive groups on the sensor's surface to undergo bond breakage. This can lead to a decrease in the quantity of active adsorption sites accessible for MB molecules to attach to. The reduction in the number of active adsorption sites also adds to the decrease in the adsorption amplitude of MB.

The presence of MB on the surface of the QCM-based Nano iron sensor leads to a significant alteration in frequency, which is attributed to the mass of MB that is adsorbed onto the sensor surfaces. The rise in temperature causes a reduction in the extent of adsorption, which in turn leads to a decrease in the amount of the observed frequency change. In general, the graph clearly demonstrates that as the temperature rises from 20°C to 25°C, the rate at which MB is adsorbed onto the surface of the mixed Schiff base iron complex sensor increases dramatically. However, at 30°C, the adsorption rate decreases due to the elevated diffusion rate of MB in the solution. The temperature dependency of this phenomenon can be ascribed to the increased kinetic energy and mobility of MB molecules at elevated temperatures, which allows for faster and more effective interactions with the sensor surface.

3.3.7. Effect of different PH

The scientific report [54] investigates the adsorption of cationic methylene blue (MB) dye onto cellulose olive stones biomass and examines its thermodynamic characteristics [63-64]. Furthermore, researchers have examined the impact of alkali on MB and other thiazine dyes [68]. The pH of the solution is a crucial factor in the dye adsorption process. When dyes are dissolved in water, they break apart and create ions, which create electric charges. Figures 10 and 11. The pH of the solution governs the magnitude and nature of the electrostatic charges emitted by the dyes.

The pH affects the adsorption of a certain dye onto an adsorbent due to the attraction of opposite charges and the repulsion of comparable charges. Adsorption of MB may decrease when the solution pH is very basic or alkaline. This is because solutions with a high pH or alkaline nature undergo a reaction with MB, a cationic thiazine dye. This reaction causes the degradation of MB^+ and the creation of methylene violet Blue. Consequently, the positive charges of MB diminish, resulting in diminished electrostatic attraction between MB and the negatively charged Nano Iron sensor.

The attenuation of the electrostatic interactions can lead to an elevation in the frequency shifts detected by the sensor. Hence, the pH of the solution plays a crucial role in the adsorption of MB onto the Nano Iron complex sensor. Elevated pH levels can result in a decline in MB adsorption due to diminished positive charges and diminished electrostatic attractions. This can lead to a rise in the frequency changes detected by the sensor, as depicted in Figure 12.

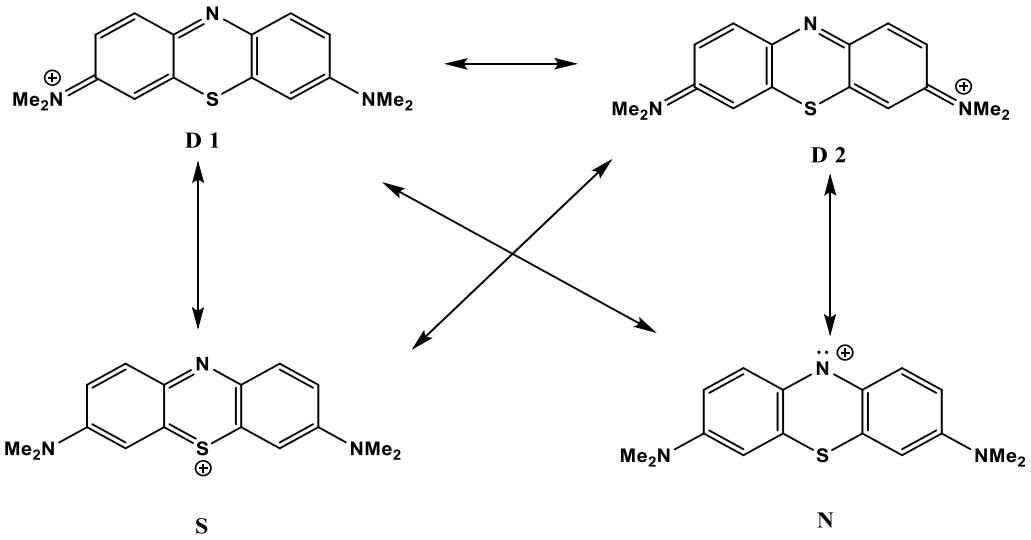

Fig 10. displays the primary valence bond resonance configurations of MB.

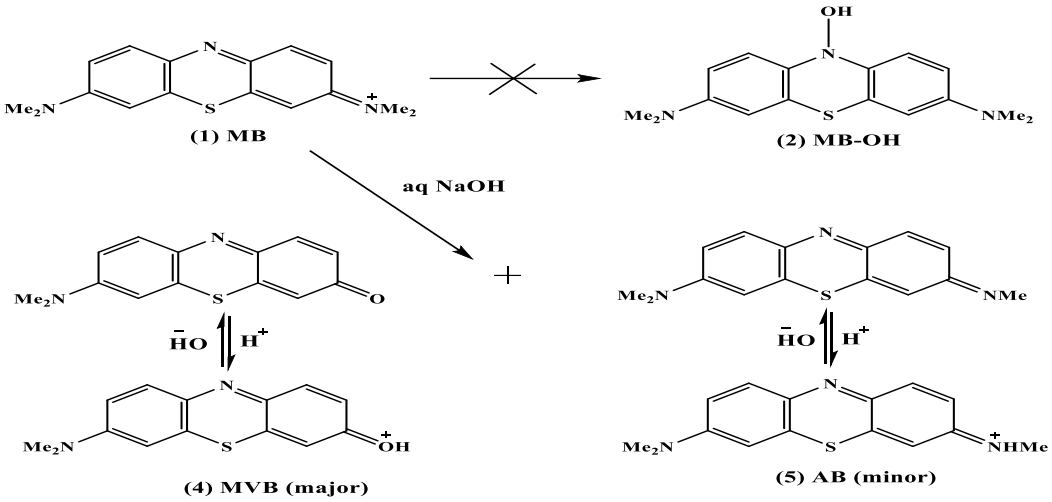

Fig 11. a concise overview of the reactions of MB in both alkaline and acidic environments.

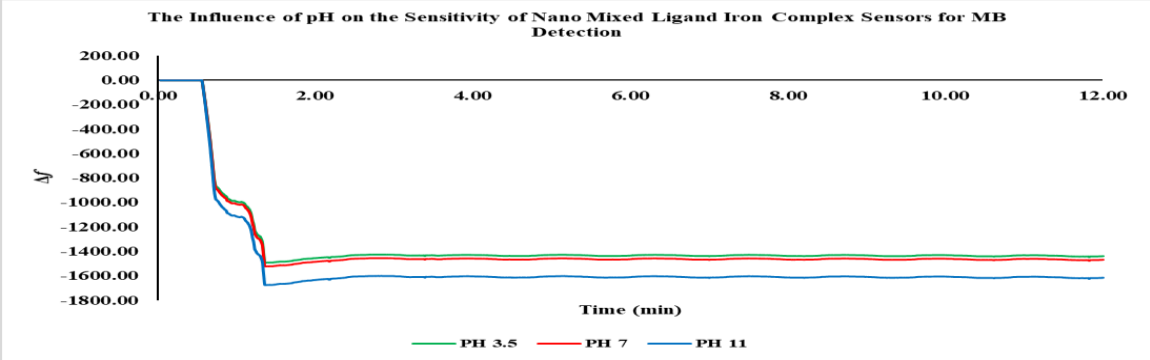

Fig 12. The Influence of pH on the Sensitivity of Nano Mixed Ligand Iron Complex Sensors for MB Detection

The graph illustrates the correlation between pH levels and the sensitivity of Nano-mixed ligand iron complex sensors in detecting methylene blue (MB) [69-70]. The adsorption of MB onto the sensor surface is influenced by the pH of the solution, as indicated by the frequency shifts recorded at pH values of 3.5, 7, and 11. At a pH of 3.5 (shown by the green line), the frequency shift demonstrates a sharp and rapid decrease, suggesting the quick adsorption of MB onto the sensor's surface. The observed behavior can be ascribed to the protonation of the mixed Schiff base iron complex at lower pH levels, leading to an augmented positive charge on the sensor surface. The electrostatic interaction between the positively charged sensor surface and the cationic MB molecules enables their effective adsorption. Additionally, there is potential for coordination between MB's nitrogen atoms and the iron center, which may become more accessible under acidic conditions. π-π stacking interactions are also likely between the aromatic rings in MB and the Schiff base complex. Furthermore, hydrogen bonding may occur between the protonated groups on the sensor and MB. Lastly, the acidic environment could facilitate possible redox reactions. The frequency shifts at a pH of 7 (shown by the red line) show a less steep decrease than a pH of 3.5, indicating a slower rate of MB adsorption onto the sensor surface. At a pH of 7, the iron complex with a mixture of Schiff bases may have a reduced positive or no charge, decreasing the electrostatic attraction with the positively charged MB molecules. There is moderate electrostatic attraction due to the overall negative zeta potential (-21) of the complex. Coordination between MB and iron may still occur, though less favorably than in acidic conditions. However, π-π stacking and hydrophobic interactions remain significant. Additionally, hydrogen bonding may occur between MB and oxygen atoms in the complex. As a result, the process of adsorption becomes slower. At a pH of 11 (shown by the blue line), the frequency shift exhibits a comparable pattern to that observed at pH 7. This suggests a rather gradual decrease, indicating a slower rate of MB adsorption onto the sensor's surface. Under alkaline conditions, the mixed Schiff base iron complex can acquire a negative charge, leading to electrostatic repulsion with the cationic MB molecules. This repulsion hinders the adsorption of the MB molecules onto the sensor surface. There is also the possibility of MB deprotonation, which would alter its charge distribution and interaction capabilities. In the absence of strong electrostatic attraction, π-π stacking and hydrophobic interactions may become more dominant. Additionally, there is potential for new coordination modes due to the altered electronic state of both the complex and MB. However, the likelihood of hydrogen bonding is reduced due to the deprotonation of sensor surface groups. In summary, the graph indicates that the adsorption of MB onto the surface of the mixed Schiff base iron complex sensor is more likely to occur in acidic circumstances (pH 3.5). The positively charged sensor surface enables effective electrostatic interactions with the cationic MB molecules. At pH levels 7 and 11, considered neutral

and alkaline, the rate at which adsorption occurs drops. This is because there is a decrease in electrostatic attraction or an increase in potential repulsion between the sensor surface and the MB molecules.

4. Conclusion

This study successfully developed an iron(II) Schiff base complex nanosensor with exceptional sensitivity and selectivity for detecting the toxic dye methylene blue (MB) using electrochemical methods. The structure and composition of the iron(II) Schiff base complex were meticulously characterized through various analytical techniques, including UV-Vis, FT-IR, NMR, mass spectrometry, elemental analysis, and thermal analysis. Following its conversion into nanoparticles, the nanoparticles were characterized by SEM, AFM, Zeta potential, and DLS analysis. The complex was then immobilized onto a quartz crystal microbalance (QCM) electrode to fabricate the nanosensor. The QCM-based nanosensor demonstrated rapid response times of less than 2 minutes for detecting MB with high sensitivity, capable of detecting concentrations as low as 1 part per million (ppm). Comprehensive performance assessments under varying temperature and pH conditions revealed that MB adsorption was enhanced at acidic pH levels due to electrostatic attractions, while adsorption decreased at highly basic pH levels. The optimal temperature for achieving the best equilibrium between diffusion and adsorption kinetics was found to be 25°C. Mechanistic studies revealed that the sensitive detection of MB was facilitated by both π-π interactions and electrostatic forces between the iron(II) complex and MB. Notably, the produced iron(II) Schiff base nanoparticles were found to be hydrophobic and non-toxic, making them environmentally sustainable for sensing applications. In conclusion, the developed nanosensor offers a promising approach for the accurate and specific real-time monitoring of toxic dyes such as MB in industrial wastewater, representing a significant advancement over conventional techniques. This innovative sensor holds potential for broader applications, suggesting that future research could explore the detection of other hazardous pollutants using this nanotechnology-enabled sensing approach.

References

1. B. Lellis, C. Z. Fávaro-polonio, J. A. Pamphile, and J. C. Polonio, "Effects of textile dyes on health and the environment and bioremediation potential of living organisms," 2019.
2. A. Patti, G. Cicala, and D. Acierno, "Eco-sustainability of the textile production: Waste recovery and current recycling in the composites world," Polymers (Basel)., vol. 13, no. 1, p. 134, 2020.
3. A. Desore and S. A. Narula, "An overview on corporate response towards sustainability issues in textile industry," Environ. Dev. Sustain., vol. 20, pp. 1439–1459, 2018.
4. M. S. Hossain, S. C. Das, J. M. M. Islam, M. A. Al Mamun, and M. A. Khan, "Reuse of textile mill ETP sludge in environmental friendly bricks–effect of gamma radiation," Radiat. Phys. Chem., vol. 151, pp. 77–83, 2018.
5. Y. Rasmi, K. S. Saloua, M. Nemati, and J. R. Choi, "Recent progress in nanotechnology for COVID-19 prevention, diagnostics and treatment," Nanomaterials, vol. 11, no. 7, p. 1788, 2021.
6. H. Wan et al., "Biomedical sensors," in Biomedical Information Technology, Elsevier, 2020, pp. 51–79.
7. S. Iyer et al., "mm-Wave radar-based vital signs monitoring and arrhythmia detection using machine learning," Sensors, vol. 22, no. 9, p. 3106, 2022.
8. K. L. Moabelo, D. R. Martin, A. O. Fadaka, N. R. S. Sibuyi, M. Meyer, and A. M. Madiehe, "Nanotechnology-based strategies for effective and rapid detection of SARS-CoV-2," Materials (Basel)., vol. 14, no. 24, p. 7851, 2021.
9. B. Santos et al., "Nanotechnology meets immunology towards a rapid diagnosis solution: the COVID-19 outbreak challenge," RSC Adv., vol. 12, no. 49, pp. 31711–31728, 2022.
10. H. Saleem, S. J. Zaidi, A. F. Ismail, and P. S. Goh, "Advances of nanomaterials for air pollution remediation and their impacts on the environment," Chemosphere, vol. 287, p. 132083, 2022.
11. H. Saleem, S. J. Zaidi, A. F. Ismail, and P. S. Goh, "Advances of nanomaterials for air pollution remediation and their impacts on the environment," Chemosphere, vol. 287, p. 132083, 2022.
12. C. Sharma, R. Dhiman, N. Rokana, and H. Panwar, "Nanotechnology: an untapped resource for food packaging," Front. Microbiol., vol. 8, p. 243298, 2017.
13. M. B. Kulkarni, N. H. Ayachit, and T. M. Aminabhavi, "Recent advances in microfluidics-based electrochemical sensors for foodborne pathogen detection," Biosensors, vol. 13, no. 2, p. 246, 2023.
14. Z. Hua, T. Yu, D. Liu, and Y. Xianyu, "Recent advances in gold nanoparticles-based biosensors for food safety detection," Biosens. Bioelectron., vol. 179, p. 113076, 2021.
15. B. Monisha, R. Sridharan, P. S. Kumar, G. Rangasamy, V. G. Krishnaswamy, and S. Subhashree, "Sensing of azo toxic dyes using nanomaterials and its health effects-A review," Chemosphere, vol. 313, p. 137614, 2023.
16. I. D. Dulama et al., "Quartz crystal microbalance used for determination of dyes from wastewaters," in CAS 2013 (International Semiconductor Conference), IEEE, 2013, pp. 107–110.
17. G. V Cimpoca et al., "Quartz Crystal Microbalance (QCM): An Alternative Analytical Method for Investigation in Real-Time of Liquid Properties," in AIP Conference Proceedings, American Institute of Physics, 2010, pp. 160–165.
18. R. Lucklum, S. Roesler, and P. Hauptmann, "On-line detection of organic pollutants in water by selective quartz crystal microbalance," Department of Commerce, National Institute of Standards and Technology …, 1996.
19. F. J. Tovar-Lopez, "Recent Progress in Micro-and Nanotechnology-Enabled Sensors for Biomedical and Environmental Challenges," Sensors, vol. 23, no. 12, p. 5406, 2023.

20. M. S. Mansour, W. H. Mahmoud, and A. A. El-Sherif, “Manganese, Cobalt, and Cadmium Complexes of Quinazoline Schiff Base Ligand and Methionine: Synthesis, Characterization, DFT, Docking studies and biomedical application,” Egypt. J. Chem., 2024.
21. G. C. Pradeep, “Protein-based functional nanoparticles: Comparison of strategies for design and engineering.” Monash University, Clayton Australia, 2018.
22. W. H. Mahmoud and A. A. El-Sherif, “Design and characterization of Nano cobalt complex as low limit detection qcm sensor for cadmium ions,” Egypt. J. Chem., 2023.
23. W. H. Mahmoud, A. A. Fayek, A. Taha, and A. A. El-Sherif, “Synthesis, textural and thermal properties of Nano super hydrophobic cupper complex as QCM based dye sensor,” Egypt. J. Chem., vol. 67, no. 4, pp. 485–494, 2024.
24. M. Okan and M. Duman, “Development of Molecularly Imprinted Polymer-based Microcantilever Sensor System,” Adv. Mol. Imprinting Mater., pp. 637–679, 2016.
25. [2] M. C. Dixon, “Quartz crystal microbalance with dissipation monitoring: enabling real-time characterization of biological materials and their interactions,” J. Biomol. Tech. JBT, vol. 19, no. 3, p. 151, 2008.
26. X.-H. Huang, W. Pan, J.-G. Hu, and Q.-S. Bai, “The exploration and confirmation of the maximum mass sensitivity of quartz crystal microbalance,” IEEE Trans. Ultrason. Ferroelectr. Freq. Control, vol. 65, no. 10, pp. 1888–1892, 2018.
27. D. Grieshaber, R. MacKenzie, J. Vörös, and E. Reimhult, “Electrochemical biosensors-sensor principles and architectures,” Sensors, vol. 8, no. 3, pp. 1400–1458, 2008.
28. W. Mahmoud, A. Fayek, A. Taha, and A. El-Sherif, “Chromium complex nanoparticles sensor for arsenic detection using QCM technique,” Egypt. J. Chem., pp. 0–0, Oct. 2023.
29. A. Bratek-Skicki, M. Sadowska, J. Maciejewska-Prończuk, and Z. Adamczyk, “Nanoparticle and bioparticle deposition kinetics: Quartz microbalance measurements,” Nanomaterials, vol. 11, no. 1, p. 145, 2021.
30. W. Al-Gethami, N. Al-Qasmi, S. H. Ismail, and A. H. Sadek, “QCM-based MgFe2O4@ CaAlg nanocomposite as a fast response nanosensor for real-time detection of methylene blue dye,” Nanomaterials, vol. 13, no. 1, p. 97, 2022.
31. M. Raudino, N. Giamblanco, C. Montis, D. Berti, G. Marletta, and P. Baglioni, “Probing the cleaning of polymeric coatings by nanostructured fluids: A QCM-D study,” Langmuir, vol. 33, no. 23, pp. 5675–5684, 2017.
32. M. M. Barsan, E. M. Pinto, and C. M. A. Brett, “Methylene blue and neutral red electropolymerisation on AuQCM and on modified AuQCM electrodes: an electrochemical and gravimetric study,” Phys. Chem. Chem. Phys., vol. 13, no. 12, pp. 5462–5471, 2011.
33. N. Liu, X. Li, X. Ma, G. Ou, and Z. Gao, “Rapid and multiple detections of staphylococcal enterotoxins by two-dimensional molecularly imprinted film-coated QCM sensor,” Sensors Actuators B Chem., vol. 191, pp. 326–331, 2014.
34. A. K. Gautam, A. Kumar, K. Sharma, and B. K. Rai, “Synthesis and structural characterization of Schiff base ligand and their metal complexes,” Orient. J. Chem., vol. 32, no. 2, p. 1249, 2016.
35. S. M. Emam, S. Bondock, and A. A. M. Aldaloa, “Schiff base coordination compounds including thiosemicarbazide derivative and 4-benzoyl-1, 3-diphenyl-5-pyrazolone: Synthesis, structural spectral characterization and biological activity,” Results Chem., vol. 5, p. 100725, 2023.
36. I. Ali, W. A. Wani, and K. Saleem, “Empirical formulae to molecular structures of metal complexes by molar conductance,” Synth. React. inorganic, Met. nano-metal Chem., vol. 43, no. 9, pp. 1162–1170, 2013.
37. A. T. A. Karim and A. A. El-Sherif, “Physicochemical studies and biological activity of mixed ligand complexes involving bivalent transition metals with a novel Schiff base and glycine as a representative amino acid,” Eur. J. Chem., vol. 5, no. 2, pp. 328–333, 2014.
38. G. R. Subhashree et al., “In vitro antioxidant, antiinflammatory and in silico molecular docking studies of thiosemicarbazones,” J. Mol. Struct., vol. 1145, pp. 160–169, 2017.
39. A. A. El-Sherif, M. M. Shoukry, and M. M. A. Abd-Elgawad, “Protonation equilibria of some selected α-amino acids in DMSO–water mixture and their Cu (II)-complexes,” J. Solution Chem., vol. 42, pp. 412–427, 2013.
40. M. S. A. Mansour, A. T. Abd-Elkarim, W. H. Mahmoud, and A. A. El-Sherif, “Quinazoline-Glycine Manganese (II) Nano-Complex for Arsenic Sensing via QCM: Synthesis, Characterization, DFT Studies, Biological Evaluation and Environmental Application,” Egypt. J. Chem., 2024.
41. L. Bellamy, The infra-red spectra of complex molecules. Springer Science & Business Media, 2013.
42. D. M. Wiles, B. A. Gingras, and T. Suprunchuk, “The C= S stretching vibration in the infrared spectra of some thiosemicarbazones,” Can. J. Chem., vol. 45, no. 5, pp. 469–473, 1967.
43. K. Swaminathan and H. Irving, “Infra-red absorption spectra of complexes of thiourea,” J. Inorg. Nucl. Chem., vol. 26, no. 7, pp. 1291–1294, 1964.
44. Jain, A. K., Singh, R. K., Jain, S., & Raisoni, J. (2008). Copper (II) ion selective electrode based on a newly synthesized Schiff-base chelate. Transition Metal Chemistry, 33, 243–249.
45. Mohamed, G. G., Omar, M. M., & Ibrahim, A. A. (2009). Biological activity studies on metal complexes of novel tridentate Schiff base ligand. Spectroscopic and thermal characterization. European Journal of Medicinal Chemistry, 44(12), 4801–4812.
46. Jain, A. K., Singh, R. K., Jain, S., & Raisoni, J. (2008). Copper (II) ion selective electrode based on a newly synthesized Schiff-base chelate. Transition Metal Chemistry, 33, 243–249.

47. Mohammadi, K., Azad, S. S., & Amoozegar, A. (2015). New tetradentate Schiff bases of 2-amino-3, 5-dibromobenzaldehyde with aliphatic diamines and their metal complexes: Synthesis, characterization and thermal stability. Spectrochimica Acta Part A: Molecular and Biomolecular Spectroscopy, 146, 221–227.
48. Z. H. Abd El-Wahab, M. M. Mashaly, A. A. Salman, B. A. El-Shetary, and A. A. Faheim, "Co (II), Ce (III) and UO2 (VI) bis-salicylatothiosemicarbazide complexes: binary and ternary complexes, thermal studies and antimicrobial activity," Spectrochim. Acta Part A Mol. Biomol. Spectrosc., vol. 60, no. 12, pp. 2861–2873, 2004.
49. J. A. Smith, "Characterization of copper complex nanoparticles using scanning electron microscopy and transmission electron microscopy," J. Nanoparticle Res., vol. 45, no. 3, pp. 120–135, 2022.
50. T. I. de Menezes, R. de Oliveira Costa, R. N. F. Sanches, D. de Oliveira Silva, and R. L. S. R. Santos, "Preparation and characterization of dithiocarbazate Schiff base–loaded poly (lactic acid) nanoparticles and analytical validation for drug quantification," Colloid Polym. Sci., vol. 297, pp. 1465–1475, 2019.
51. S. Kannaiyan, Easwaramoorthy, K. Kannan, and V. Andal, "Synthesis, Characterisation, and Antimicrobial Efficacy of Acid Fuchsin Schiff Base-Modified Silver Nanoparticles," Nanotechnologies Russ., vol. 15, no. 11, pp. 828–836, 2020.
52. Tian, Y., Chen, Q., Yan, C., Deng, H., & He, Y. (2020). Classification of adsorption isotherm curves for shale based on pore structure. Petrophysics, 61(05), 417–433.
53. Van Der Voort, P., Leus, K., & De Canck, E. (2019). Introduction to porous materials. John Wiley & Sons.
54. Gao, Z., Ding, C., Wang, J., Ding, G., Xue, Y., Zhang, Y., Zhang, K., Liu, P., & Gao, X. (2019). Cobalt nanoparticles packaged into nitrogen-doped porous carbon derived from metal-organic framework nanocrystals for hydrogen production by hydrolysis of sodium borohydride. International Journal of Hydrogen Energy, 44(16), 8365–8375.
55. Wei, Y., Zhao, Z., Li, T., Liu, J., Duan, A., & Jiang, G. (2014). The novel catalysts of truncated polyhedron Pt nanoparticles supported on three-dimensionally ordered macroporous oxides (Mn, Fe, Co, Ni, Cu) with nanoporous walls for soot combustion. Applied Catalysis B: Environmental, 146, 57–70.
56. Szafraniec, M., & Barnat-Hunek, D. (2020). Evaluation of the contact angle and wettability of hydrophobised lightweight concrete with sawdust. Budownictwo i Architektura, 19(2).
57. Gavande, S. S., Navale, Y. H., Salunkhe, A. S., Gavande, S., Kulkarni, P. S., & Karche, B. R. (2020). Investigation of Supercapacitive Behaviour of Electrodeposited Cobalt Oxide Thin Film by Potentiostatic Mode. Journal of Nano-and Electronic Physics, 12(2).
58. Sayed, M. M., Nabil, Z. I., El-Shenawy, N. S., Al-Eisa, R. A., & Nafie, M. S. (2023). In Vitro and In Vivo Effects of Synthesis Novel Phenoxyacetamide Derivatives as Potent Apoptotic Inducer against HepG2 Cells through PARP-1 Inhibition. Pharmaceuticals, 16(11), 1524.
59. Nagy, E. T., Ahmed, A. A. S., Elmongy, E. I., El-Gendy, S. M., Elmadbouh, I., El Sayed, I. E. T., Abd Eldaim, M. A., & El-Gokha, A. A. (2023). Design and cytotoxic evaluation via apoptotic and antiproliferative activity for novel 11 (4-aminophenylamino) neocryptolepine on hepatocellular and colorectal cancer cells. Apoptosis, 28(3–4), 653–668.
60. N. A. A. Qasem, R. H. Mohammed, and D. U. Lawal, "Removal of heavy metal ions from wastewater: A comprehensive and critical review," Npj Clean Water, vol. 4, no. 1, p. 36, 2021.
61. S. Banerjee and M. C. Chattopadhyaya, "Adsorption characteristics for the removal of a toxic dye, tartrazine from aqueous solutions by a low cost agricultural by-product," Arab. J. Chem., vol. 10, pp. S1629–S1638, 2017.
62. M. Bahrami, M. J. Amiri, S. Rajabi, and M. Mahmoudi, "The removal of methylene blue from aqueous solutions by polyethylene microplastics: Modeling batch adsorption using random forest regression," Alexandria Eng. J., vol. 95, pp. 101–113, 2024.
63. A. A. B. Christus, P. Panneerselvam, and A. Ravikumar, "Novel, sensitive and selective colorimetric detection of arsenate in aqueous solution by a Fenton-like reaction of Fe 3 O 4 nanoparticles," Anal. methods, vol. 10, no. 36, pp. 4378–4386, 2018.
64. X.-S. Hu, R. Liang, and G. Sun, "Super-adsorbent hydrogel for removal of methylene blue dye from aqueous solution," J. Mater. Chem. A, vol. 6, no. 36, pp. 17612–17624, 2018.
65. Hassan, M. R., & Aly, M. I. (2021). Magnetically synthesized MnFe2O4 nanoparticles as an effective adsorbent for lead ions removal from an aqueous solution. AQUA—Water Infrastructure, Ecosystems and Society, 70(6), 901–920.
66. Chaabane, L., Beyou, E., El Ghali, A., & Baouab, M. H. V. (2020). Comparative studies on the adsorption of metal ions from aqueous solutions using various functionalized graphene oxide sheets as supported adsorbents. Journal of Hazardous Materials, 389, 121839.
67. Mills, A., Hazafy, D., Parkinson, J., Tuttle, T., & Hutchings, M. G. (2011). Effect of alkali on methylene blue (CI Basic Blue 9) and other thiazine dyes. Dyes and Pigments, 88(2), 149–155.
68. Al-Ghouti, M. A., & Al-Absi, R. S. (2020). Mechanistic understanding of the adsorption and thermodynamic aspects of cationic methylene blue dye onto cellulosic olive stones biomass from wastewater. Scientific Reports, 10(1), 15928.
69. Baalousha, M., & Lead, J. (2015). Characterization of nanomaterials in complex environmental and biological media. Elsevier.
70. Yang, X., Wan, Y., Zheng, Y., He, F., Yu, Z., Huang, J., Wang, H., Ok, Y. S., Jiang, Y., & Gao, B. (2019). Surface functional groups of carbon-based adsorbents and their roles in the removal of heavy metals from aqueous solutions: a critical review. Chemical Engineering Journal, 366, 608–621.